Journal of Polymers and the Environment (2022) 30:3483–3494
https://doi.org/10.1007/s10924-022-02450-0

ORIGINAL PAPER

Development of Luminescent Solution Blown Spun Nanofibers from Recycled Polyester Waste Toward Dual-mode Fluorescent Photochromism

Mohamed El-Newehy[1] · Meera Moydeen Abdulhameed[1] · Abdulnasser M. Karami[1] · Hany El-Hamshary[1]

Accepted: 1 April 2022 / Published online: 21 April 2022

Abstract

Photochromism is an interesting approach to improve the anticounterfeiting of various commercial commodities. To introduce a transparent anticounterfeiting nanocomposite, it has been crucial to enhance the engineering processing of the anticounterfeiting materials. In this context, we introduce highly phosphorescent rare-earth aluminate nano-sized particles (REAN)/recycled polyester waste (PET) nanofibrous films by solution blowing spinning for anticounterfeiting purposes. The composite nanofibers demonstrated UV-motivated photochromic anticounterfeiting performance. To warranty the translucent property of REAN@PET, it is necessary to immobilize REA in the nano-sized form for an improved dispersion without agglomeration in the polyester nanofibrous bulk. Various nanofibers films of diverse emission characteristics were developed employing various ratios of REAN. Transmission electron microscopy and X-ray diffraction were utilized to determine the morphology of REAN to demonstrate diameters of 4–9 nm. The energy-dispersive X-ray analysis, infrared spectra, X-ray fluorescent analysis, elemental mapping, and scanning electron microscope were employed to study the morphologies, optical transmittance, elemental contents, and mechanical properties of the prepared photo-induced chromic nanofibers. The nanofiber diameter in the REAN@PET film was reported in the range of 180–220 nm. The REAN@PET nanofibrous film demonstrated an excitation band at 365 nm in association with an emission band at 519 nm. The solution blown spun REAN@PET nanofibrous films showed an improved superhydrophobicity with raising the REAN content. When excited under UV supply, the transparent nanofibers showed a rapid and reversible dual-mode fluorescent photochromism to green without fatigue. The present anti-counterfeiting films can be reported as a simple and effective approach to build versatile materials to introduce an ideal marketplace with economical and community benefits at low-cost.

Keywords Rare-earth aluminate · Polyester · Solution blown spun nanofibers · Photochromism · Dual-mode authentication

Introduction

There has been an increase in the number of counterfeit and low-quality items in many contemporary commodity industries, which poses a serious danger to the community. As a result, there has been an ever-increasing need for the creation of innovative anti-counterfeiting materials that are difficult to replicate and simple to detect [1]. Various counterfeiting methods have been reported including ink, paper and digital technology. Holographic labeling, radio frequency ID, and rapid responsive encodes are all examples of modern anti-counterfeiting technology. However, these models' preparation and identification need the use of high-tech and expensive equipment, which limits their applications [2]. Recently, photochromic anti-counterfeiting films have been used in numerous products. The stimuli-responsive photoswitchable materials are known as photochromic compounds with an ability to change color when exposed to light. There have been two types of photochromic materials, including ultraviolet and visible light induced color switchable materials [3]. A wide range of products, including displays, security prints, sensors, electronic memories, ophthalmic lenses, packaging, and optical data storage have been presented using the photochromic technique [4]. It is possible to use photochromic materials in composites to build smart commodities [5]. An UV-motivated chromic film appears

✉ Mohamed El-Newehy
melnewehy@ksu.edu.sa

[1] Department of Chemistry, College of Science, King Saud University, P.O. Box 2455, Riyadh 11451, Saudi Arabia

colorless in normal daylight, but when exposed to ultraviolet light, it changes color to reveal a previously designed anti-counterfeiting model. Thus, UV-induced photochromic films have unique and innovative aesthetic effects, as well as an anticounterfeiting function [6]. These anticounterfeiting photochromic films must have an efficient optical performance, rapid responsiveness and original water vapor barrier in order to be used for the packaging of diverse commodities. The production procedures of photochromic composite films have been extensively explored at both material and matrix levels [7].

The antenna effect with ligands, long stokes displacement, high luminosity, and strong emission spectral properties of the lanthanide-doped photoluminescent materials made them good candidates for anti-counterfeiting applications. The rare-earth doped aluminate (REA; $SrAl_2O_4:Eu^{2+}$, Dy^{3+}) is a phosphor that has been widely used in luminescence applications [8]. REA is used in a number of products, including safety markings, illuminating decorative items, decorations and signage. This is due to the fact that REA has excellent photostability, long-lasting luminescence, durability, and bright luminosity [9]. Various lanthanide-doped phosphors that emit distinct primary colors have been previously reported such as $MgAl_2O_4:Mn^{2+}$ and $SrAl_2O_4:Eu^{2+}$, Dy^{3+} for green emission, $CaS:Eu^{2+}$, Tm^{3+}, Ce^{3+} and $Y_2O_2S:Eu^{3+}$, Mg^{2+}, Ti^{4+} for red emission, as well as $CaAl_2O_4:Eu^{2+}$, Nd^{3+} and $CaMgSi_2O_6:Eu^{2+}$, Dy^{3+} for bluish emission [10]. REA is one of the greatest long-lasting phosphors because it is nontoxic, chemical and solvent resistant, nonradioactive, heat and water resistant, photostable with a long-lasting emission (> 10 h), and recyclable [11]. As a result, the preparation of UV-motivated photochromic REA-loaded polyester nanofibers is a new attractive technology with low cost, photostability and high durability, and enhanced hydrophobicity, which introduces novel horizons for the development of more stable and effective smart commodities. However, REA's chemical and physical properties, as well as its particle moulding, are often unsuitable for engineering purposes, limiting its uses [12]. Thus, the REA complex has been integrated into various organic and inorganic substances to defeat their limited mechanical stability. Nano-sized materials were proved to exhibit high capability to uphold the transparent appearance of various products. Thus, it has been significant to apply the pigment phosphor in the nanostructure form; rare-earth doped aluminate nanoparticles (REAN) [13].

Polyethylene terephthalate (PET), a kind of polyester, is one of the most important polymers having an ester repeating unit. Biodegradable polyesters include those derived from plants and a small percentage of synthetic polyesters; however, the majority of synthetic polyesters are not biodegradable. The production of knitted and woven textiles using synthetic PET has become widespread [14]. In a variety of applications, high-performance PET fibers have been employed in a variety of applications including textiles, adhesives, safety belt fabrics, tarpaulins, as well as bottles, canoes and sails. Dielectric films, insulators, capacitors, filtration systems, and holograms have all been made of polyester [15, 16]. The liquid crystalline PET was one of the first liquid crystalline polymers to be used in electronic displays in industry. PET films exhibit resistance to chemicals, heat, water and ageing as well as excellent mechanical properties. Shredding recycled PET bottles to remove excess fluids does not impact the integrity of the plastic. It is possible to take away the colored contents and stickers from the shredded plastics in order to produce clear plastics, which are subsequently charged into a hot bath in the refinery process. A transparent plastic shred makes up the remaining mass [17, 18]. PET's low heat conductivity, minimal shrinkage upon curing, shatterproof characteristics, mechanical durability, cheap cost, and excellent optical transmittance have lately gained major interest. In other words, PET is a useful bulk material for various anti-counterfeiting applications [19]. However, only a few studies have been reported for the preparation and application of PET-based photochromic materials. Thus, the incorporation of REA into polyester substrates for the preparation of anticounterfeiting goods has proven noteworthy.

Smart nanofibers have been used to make wearable sensors for medical applications and electronic displays [20]. Using electrospinning, REA complexes have been integrated into polymeric materials to produce nanofibers with great luminescence effectiveness and strong mechanical stability. For instance, stretchable and wearable electronics may benefit from large-scale fabrication of multicolor photoluminescent core-shell nanofibrous films based on perovskite/PET. However, electrospinning produces nanofibers that are expensive, need a high voltage, and often produce nanofibers in a limited yield. To make the matter more complicated, only viscoelastic materials can be used for electrospinning [21, 22]. Because it does not need the use of high voltage like electrospinning, the newly developed solution blowing spinning has shown to be simpler to operate, less expensive, more productive, and safer technology [22, 23]. The inclusion of REAN into PET matrix has not yet been documented yet. Additionally, the application of the solution blowing spinning technology to generate nanofibers from recycled polyester wastes has not been reported yet. Herein, the current manuscript describes the preparation of photoluminescent nanofibers from recycled polyester wastes using solution blowing spinning technology toward dual-mode fluorescent photochromism for anticounterfeiting authentication. For anti-counterfeiting purposes, we have developed a simple method to produce REAN@PET nanofibrous photochromic film. The morphological features, mechanical performance, and photoluminescence, were examined. Both

sliding and contacting angle measurements were studied to show an improved hydrophobicity without significantly impacting the inherent physico-mechanical properties of the produced nanofibrous films. The REA nanoparticles were found to be completely incorporated in the PET matrix. The created nanofibrous films were flexible, pliable, and translucent. Stability under a variety of tensile loads was an indicator of the capacity to stretch-resiliently. An anti-counterfeit mark is ideal for luminous transparent films since they are UV-induced photochromic materials. The colorimetric characteristics were explored by the CIE Lab to demonstrate that such a counterfeiting model appears in a green color beneath ultraviolet light with no traces under visible light.

Experimental Section

Materials and Reagents

N,*N*-dimethylformamide (DMF, ≥ 99%) and polyethylene glycol (PEG) 400 were purchased from Sigma-Aldrich (Egypt). Shredded polyester waste was supplied from aquahgroup, Egypt. In order to prepare the REA pigment, the solid-state high temperature approach was applied [24]. The compounds used in the synthesis of REA include dysprosium oxide (Aldrich), H_3BO_3 (Merck), aluminum oxide (Merck), europium oxide (Aldrich), strontium carbonate (Merck), and absolute ethanol (Merck).

Synthesis of REAN

Solid-state high-temperature technique was used to synthesize the REA ($SrAl_2O_4$:Eu^{2+}, Dy^{3+}) phosphor. A mixture of aluminum oxide (2.0 mol), H_3BO_3 (0.2 mol), dysprosium oxide (0.03 mol), strontium carbonate (1.0 mol) and europium oxide (0.02 mol) was dispersed in ethyl alcohol for 60 min, homogenized at 25 kHz for 60 min, subjected to drying at 90 °C, and grinded for 2 h using planetary ball mill. The given powder was sintered at 1300 °C for 3 h in a reductive carbon atmosphere. To produce REA microparticles, a sieve process was used to separate the tiny microparticles. In order to synthesize the nano-sized particles of REA, ES80 Triple Roll Mill was applied using the top-down procedure [25]. On a vibrating tablet, a stainless steel vial containing 10.0 g of REA micro-sized fine particles was subjected to repetitive collisions 24 h with a SiC ball mill to give the desired REAN.

Preparation of REAN@PET Nanofibers

In order to remove the stickers, caps, and colored substrates from the recycled PET bottles, the shredded PET bottles were charged into a hot bath at 270 °C as a refinery process to provide transparent plastics. The plastic shreds (15 g/L) were well-mixed with pure PET (20 wt%), PEG (1.5 wt%; plasticizer) and REAN in DMF under mechanical stirring for 2–3 h until the mixture became homogenous as indicated by the solution color change to colorless, which indicated the disappearance of REAN aggregates. The REAN@PET nanofibrous films were prepared by charging the above-prepared viscous solutions into the solution blowing spinning tool. The components of the solution blowing spinning tool, includes a collector, injection pump, spinning nozzle and air compressor. A spin needle was used to inject the REAN@PET viscous solution at a 8 mL/h flow rate and a 0.5 bar air pressure. The collector was maintained about 10 cm from the spinning nozzle. The spin needle was set at the concentre nozzle center, and the protrusion was performed at a distance of 1 mm from the concentric nozzle. The REAN@PET nanofibrous films were prepared using various ratios of REAN, including 0, 0.1, 0.25, 0.5, 0.75, 1, 1.25, and 1.5%. The symbols from NF-0 to NF-7, respectively, were used to represent the generated nanofibers. The resulting REAN@PET fibrous films had a 1.5 cm width, a 2.5 cm length, and a thickness of ~ 30 μm.

Analytical Methods

Morphologies and Elemental Compositions

SEM (Quanta FEG-250; Czech) coupled with TEAM EDX was used to examine the morphological characteristics and elemental contents of REAN@PET. To determine the diameters of REAN@PET nanofibers, Image J software set up on SEM was used. The REAN was examined using JEOL1230 transmission electron microscope (TEM; Japan). XRD pattern of REAN was inspected at a 2θ (Bragg angle) of 10°–80°, using Bruker Advance D8 (Germany). A Nexus 670 spectrophotometer (Nicolet; United States) was used to collect FT-IR spectra.

Mechanical Properties

AGX Shimadzu (Japan) with a 100 N load cell was employed to obtain the mechanical measurements [26].

Hydrophobic Properties

Dataphysics OCA15EC (GmbH, Germany) was used to analyze the contact angle data [26].

Luminescence Spectra

The photoluminescence measurements were made using a JASCO FP-8300 spectrofluorometer (Japan) connected with phosphorescence accessories. At 365 nm, a 6 W

ultraviolet device was used as an UV source. Edinburgh FS5 fluorescence spectrophotometer was used to measure the photoluminescence quantum yields. The decaying time was determined utilizing the luminescence accessories attached to the FP8300 JASCO (Japan) spectrophotometer. After a 10 min of ultraviolet irradiation (365 nm), the persistent luminescence material optical testing equipment was used to measure the photoluminescence afterglow lifetime of the sample that had been pre-irradiated.

Photostability

By measuring the emission intensity before to and after irradiation with an ultraviolet, we were able to determine the photostability and reversibility of the REAN@PET films. When the sample was excited with ultraviolet for five min, the emission energy was released and the sample returned to its original condition after turning the UV source off. The emission (519 nm) was recorded pre-UV and post-UV irradiation over several cycles [27].

Colorimetric Study

UltraScanPro (Hunter Lab; United States) setup was used to measure the color change of REAN@PET by reporting tinctorial strength (*K/S*) and CIE Lab. The color coordinates (CIE Lab; L^*, a^* and b^*) were determined. Irradiation with an ultraviolet light was used to treat the nanofibrous films, and the pre-UV and post-UV findings were analyzed. The reflectance technique was used to measure the *K/S* values. The A710-IS digital camera took the photos of the photochromic nanofibers. HITACHI's UV-visible U-3010 spectrophotometer was used to measure the REAN@PET films' optical transmission [27].

Results and Discussion

Fabrication of Smart Fibers

To obtain REA nanoparticles, the top-down method [25] was applied on the micro-sized REA particles synthesized by the solid-state high temperature procedure [24]. Figure 1a–c depicts the 4–9 nm nanoparticle diameters that were identified by TEM. XRD pattern of the synthesized

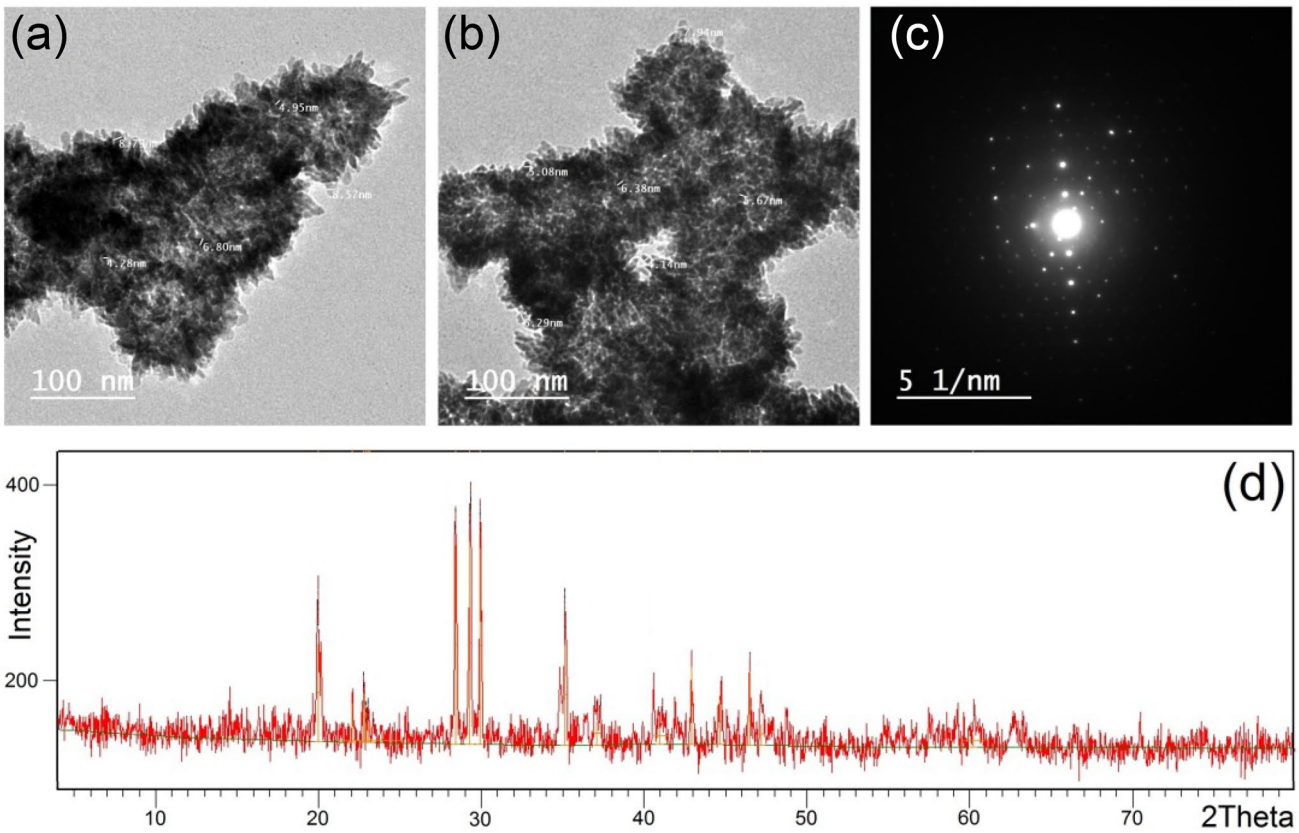

Fig. 1 TEM graphs (**a**–**c**), and XRD pattern of REAN

REAN is depicted in Fig. 1d. The diffraction peaks of REAN matched the monoclinic phase of $SrAl_2O_4$ (JCPDS card No. 74-0794). Pure monoclinic phase of $SrAl_2O_4$ were detected as no diffraction signals were observed for neither starting compounds nor other by-products to prove a low temperature monoclinic phase of the precursor nanopowder. No other crystalline phases were observed to indicate a complete inclusion of dopants (Eu^{2+} or Dy^{3+}) in the crystal lattices of $SrAl_2O_4$ [28, 29]. Shredded polyester bottles were heated at 270 °C as a refinery process to remove stickers, caps, and colored contents and provide transparent plastics. A mixture of produced transparent plastic shreds and REAN was dispersed in DMF to provide a colorless and viscous homogenous solution. The REAN@PET nanofibers were prepared using the solution blowing spinning tool.

Photoluminescence Spectra

The REAN@PET films had a transparent backdrop so that the ultraviolet–induced green shift could be better detected optically. Instant and reversible photochromism was observed in all REAN@PET films. In contrast, only REAN@PET with REAN contents lower than 1% (NF-1 to NF-5) were able to demonstrate fluorescence. As a result of their slow reversibility, the other samples with REAN ratios greater than 1% (NF-6 and NF-7) exhibited a long-lasting phosphorescence emission. The absorbance intensity of NF-5 was measured and reported at 365 nm. The emission intensities of NF-5 were reported against time ranging from 10 to 40 s after ultraviolet irradiation (Fig. 2). The wavelength of 519 nm was found to correspond to a distinct emission band, which displayed time-dependent changes at 519 nm as the emission intensity increased with

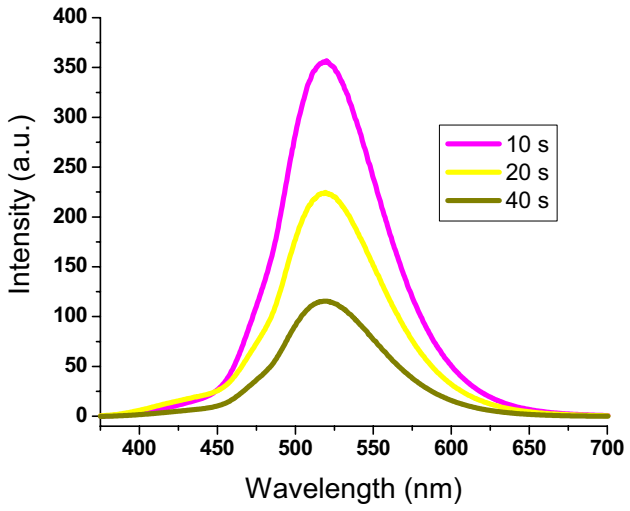

Fig. 2 Fluorescence spectra of REAN@PET film (NF-5) versus the excitation time (10–40 s)

increasing the irradiation time under an UV lamp. Similarly, the emission intensities of the REAN@PET films displayed concentration-dependent changes at 519 nm as the emission intensity increased with raising REAN. The interpolymeric strands of polyester were strengthened by the REA nanoparticles via physical entrapment of REAN in the polyester bulk, which results in coordination bonding of the positive aluminum ions in REAN with the partially negatively charged polyester carbonyl and hydroxyl oxygen atoms [30, 31].

Figure 2 shows the photoluminescence spectra of the nanofibrous REAN@PET film (NF-5) demonstrating a strong green emission at 519 nm. The 4*f*-5*d* transition of Eu(II) is responsible for those peaks [32]. It is thought that two strontium sites could be found in the $SrAl_2O_4$ crystal structure. However, the thermal quenching of the blue emission peak at ambient circumstances makes the bluish peak weaker [33]. As a result, only the most prominent greenish emission could be observed. The luminescence spectra did not show the emission of the trivalent europium. Consequently, only the divalent europium ions are responsible for the photoluminescence. The decreasing concentration of REAN is a primary factor in the reduced photoluminescence intensity. The quantum yield (QY) of REAN@PET was calculated using the integrating sphere method [34]. The quantum yields of the REAN@PET films with the lowest and highest concentrations of REAN ranged between 10% and 50%, respectively. Because of this, the quantum yield of the REAN@PET films is lower than that of the solid REA nanpowder (85%) due to the ability of the polyester bulk to block the incident and emitted light leading to decreasing the numbers of the absorbed and emitted light photons. The decay time of the REAN@PET films were recorded (Fig. 3). All decay spectra followed an exponential second-order decaying according to Eq. (1) [35].

$$I(t) = A_1 \exp\left(\frac{-t}{\tau_1}\right) + A_2 \exp\left(\frac{-t}{\tau_2}\right), \quad (1)$$

where t, τ_1 and τ_2 represents decaying time, I is initial luminescence intensity, and A_1 and A_2 are constants.

The average life-time (τ_{ave}) was estimated according to Eq. (2) [36].

$$\tau_{ave} = \frac{A_1(\tau_1)^2 + A_2(\tau_2)^2}{A_1\tau_1 + A_2\tau_2} \quad (2)$$

Depending on Eq. (2), the τ_{ave} value of REAN is 865.2 μs, and τ_{ave} of the REAN@PET films increased in the range of 241.9–287.1 μs with raising the REAN ratio. This proves that the insertion of REAN in the polyester matrix leads to shorter lifetime for the REA nanoparticles trapped in the polyester matrix. The corresponding decrease in the

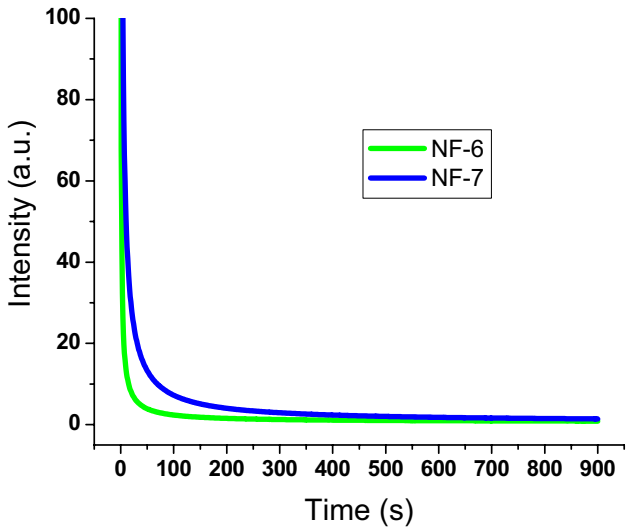

Fig. 3 Decay time spectra of REAN@PET at 519 nm

quantum yields of the REAN@PET films also accounts for the reduced lifetime according to Eq. (3) [37].

$$QY = \frac{1/\tau_r}{(1/\tau_r) + (1/\tau_{nr})} = \frac{1/\tau_r}{1/\tau_{ave}} = \frac{\tau_{ave}}{\tau_r}, \quad (3)$$

where r and nr (r is constant) are the radiative and non-radiative decays, respectively. The quantum yield is proportional to τ_{ave}. The relationship of the quantum yield to τ_{ave} of REAN and REAN@PET can be converted using Eq. (4) [37].

$$\frac{QY\,(REAN)}{QY\,(REAN@PET)} = \frac{\tau_{ave}(REAN)}{\tau_{ave}(REAN@PET)} \quad (4)$$

Consequently, the QY of REAN was about three times more than that of REAN@PET. Using the integration sphere technique, we found that our testing findings were quite close to this. When exposed to UV light for 10 min at 365 nm, the luminous life-time of REAN and REAN@PET was almost identical. REAN displayed a long-persistent luminous lifetime of up to 10 s, whereas REAN@PET nanofibrous films have a long-persistent luminescent lifetime of up to 5 s after terminating UV irradiation. The lifetime of REAN@PET was monitored to increase (0–5 s) with increasing the ratio of REAN.

Coloration Measurements

Table 1 summarizes the photochromic colorimetric characteristics. All REAN-immobilized polyester samples had a transparent appearance. Because the REAN phosphor is immobilized by physical dispersion, the transparent REAN@PET film can only be formed if it is evenly distributed. As a result of their exceptional capacity to preserve the transparency of various commodities, nanomaterials have become critical substrates in the manufacturing of transparent materials. Under UV light, a green fluorescence emission was proved by CIE Lab findings for films with lower ratios of REAN less than NF-5. On the other hand, a long-lasting green phosphorescence emission was monitored for the REAN ratios of NF-6 to NF-7. The *K/S* changes were insignificant when increasing the REAN ratio from NF-0 to NF-7, confirming the transparency of the films due to their low nano-sized REA concentrations. The *K/S* was then increased upon switching the incident light from visible to ultraviolet indicating a color change from colorless to greenish-yellow. However, when the REAN concentration increased from NF-5 to NF-7, only small variations in *K/S* were detected. The REAN@PET film under UV radiation had a *K/S* ratio higher than that of the same unirradiated film, leading to greener hues depending on the REAN ratio as the intensity of the emission was monitored to increase with increasing the ratio of REAN indicating a greener color. The excitation maxima of the REAN@PET films detected at 365 nm indicating a transparent appearance, and the emission wavelength was detected at 519 nm indicating a green color. The NF-0 film showed no changes in the CIE Lab parameters between the visible and UV lights. The L^*, a^*, and b^* values of the photoluminescent REAN@PET films changed significantly when REAN was increased. When exposed to natural light, L^* dropped from NF-1 to NF-7, indicating reduced transparency and giving the samples a

Table 1 Colorimetric properties of REAN@PET under Vis and UV lights

Parameter		NF-0	NF-2	NF-1	NF-3	NF-4	NF-5	NF-6	NF-7
K/S	Vis	0.26	0.31	0.46	0.52	0.58	0.73	1.12	1.68
	UV	0.38	1.54	1.64	1.77	1.89	1.97	2.33	2.95
L^*	Vis	89.93	88.55	86.63	85.73	85.06	83.38	82.97	82.23
	UV	90.05	84.68	83.55	81.25	80.38	78.62	76.95	75.43
a^*	Vis	− 1.84	− 2.29	− 2.15	− 1.98	− 1.71	− 1.60	− 1.04	− 0.66
	UV	− 1.90	− 5.20	− 5.86	− 6.58	− 7.23	− 7.92	− 8.62	− 9.37
b^*	Vis	1.38	1.06	0.95	0.84	0.72	0.56	0.55	0.42
	UV	1.45	11.62	11.76	10.89	8.66	7.34	6.70	6.18

slightly off-white color. L^* decreased from NF-1 to NF-7 under UV light owing to the greener shade that was reported with increasing the REAN ratio. The UV radiation caused a change in colorimetric values from transparent to green by increasing the value of $-a^*$ and decreasing the value of $+b^*$. The films from NF-1 to NF-5 returned immediately to its origin transparent non-emissive status after the UV device was turned off indicating fluorescence emission. It has been shown that the long-lasting phosphorescence is associated with a decrease in $+b^*$ and an increment in $-a^*$ in films with higher REAN ratios (NF-6 and NF-7). These findings show that NF-5 has the most fitting photochromism.

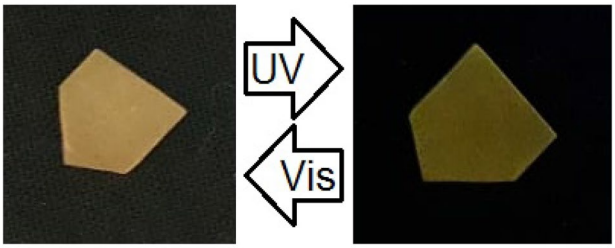

Fig. 4 Photographs taken under daytime (*left*) and ultraviolet (*right*) lights showing a printed design with transparent and green color, respectively

Photochromic Measurements

For anti-counterfeiting purposes, the UV-promoted luminescent materials have been frequently used. However, the use of photochromic plastic-based films has been limited. Herein, a transparent film with dual-mode fluorescent photochromism was formed from a combination of REAN with transparent polyester to generate nanofibers using the solution blowing spinning method. The photochromic activity was accomplished by embedding REAN in the transparent PET film. However, under UV irradiation, it produces a vivid greenish-yellow hue that can be seen with the human eye. Currently, the anti-counterfeiting procedures used in cosmetic items rely on traditional approaches, in which distinct anticounterfeiting prints were used as patterns. Because of this, it's possible that high-end brand cosmetics get tainted by subpar or counterfeit goods. In order to use the REAN@PET film, we created a gasket. An impregnated rectangular form could be used as a model. The product's gasket is transparent and the pattern is invisible to the naked-eye; but, under UV irradiation, it emits a green color that cannot be copied. The REAN@PET film was glued over a plastic bottle sign in order to produce additional packaging prototypes. The sign was invisible to the human eye under normal light, and was able to produce a greenish color when exposed to UV light, showing the principle of UV-induced anticounterfeiting authentication. UV-induced anti-counterfeiting prototype for packaging purposes is demonstrated in Fig. 4.

Photostability and Reversibility

The $4f^6 5D^1 \leftrightarrow 4f^7$ transition of Eu^{2+} is responsible for REAN's emission curves. For Eu^{3+} or Dy^{3+}, no distinctive emssions were monitored to establish that Eu(III) had fully exchanged to Eu(II). The purpose of Dy^{3+} is to stimulate the development of traps. When these traps are freed in the dark, they are transferred to Eu^{2+}, which eventually returns to its ground state [32]. The fatigue-resistant anti-counterfeiting products are very significalt to confirm photostability and durability. Over numerous cycles, it was thus necessary to test the reversibility of a coloration and decoloration processes underneath UV and visible lights, respectivley. As shown in Fig. 5, the developed samples indicated high reversibility without fatigue.

Morphological Properties

Figure 6 shows the morphological features and elemental compositions of the polyester nanofibers loaded with REAN (REAN@PET). There were no significant changes monitored between the blank NF-0 and REAN-immobilized polyester (NF-1 to NF-7). All samples showed a smooth surface with a nanofiber average diameter in the range of 180–220 nm. There were no visible REA nanoparticles on the nanofibers' surfaces to indicate that the REAN is completely encased inside the PET fiber. The analysis of the REAN@PET's elemental composition using EDX spectra confirmed the presence of RESA in the nanofibrous matrix (Table 2). The elemental distribution on the REAN@PET nanofibers was investigated by EDX to reveal a homogenous distribution of $SrAl_2O_4$ with a trace doping of Eu^{2+} and Dy^{3+}. Aluminium, europium, oxygen, strontium, carbon, and dysprosium were detected in the REAN@PET film by EDX analysis. Table 2 shows the chemical compositions of three tested places on the examined film surface. The findings showed that the elemental compositions at the three sites were almost identical to verify that REAN was consistently distributed in the REAN@PET nanofibrous film. RESA dispersion in the nanofiber matrix was further verified using the elemental mapping technique.

XRF was applied to inspect the elemental contents of the REAN@PET nanofibers as illustrated in Table 3. The elemental contents of a material could be evaluated with high accuracy utilizing the EDX analysis, which is distinguished with low error. XRF has been also employed to evaluate the chemical compositions of a material with elemental concentrations higher than 10^{-3} g/kg. As a result, XRF can recognize the chemical compositions for a limited number of materials in comparison to EDX data. Both Sr and Al were recognized in the REAN@PET nanofibers; however, Eu and

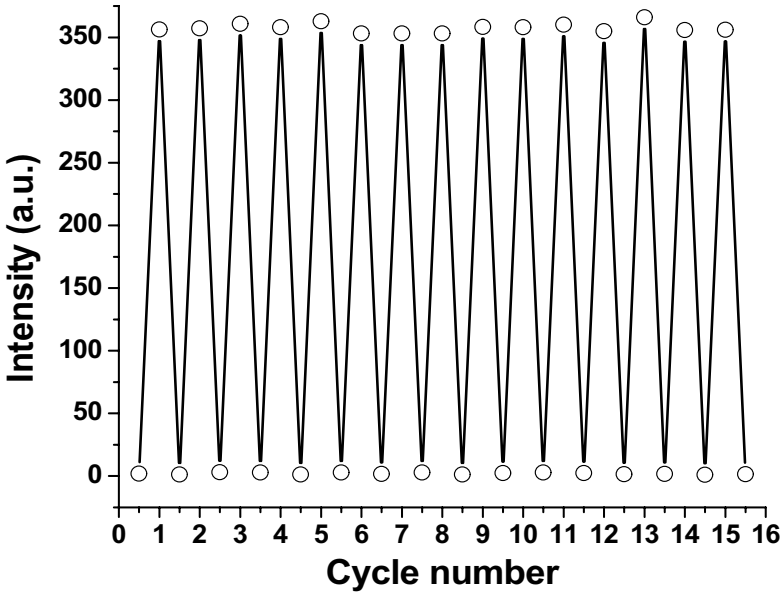

Fig. 5 Reversibility of REAN@PET (NF-5) emission at 519 nm before and under UV light

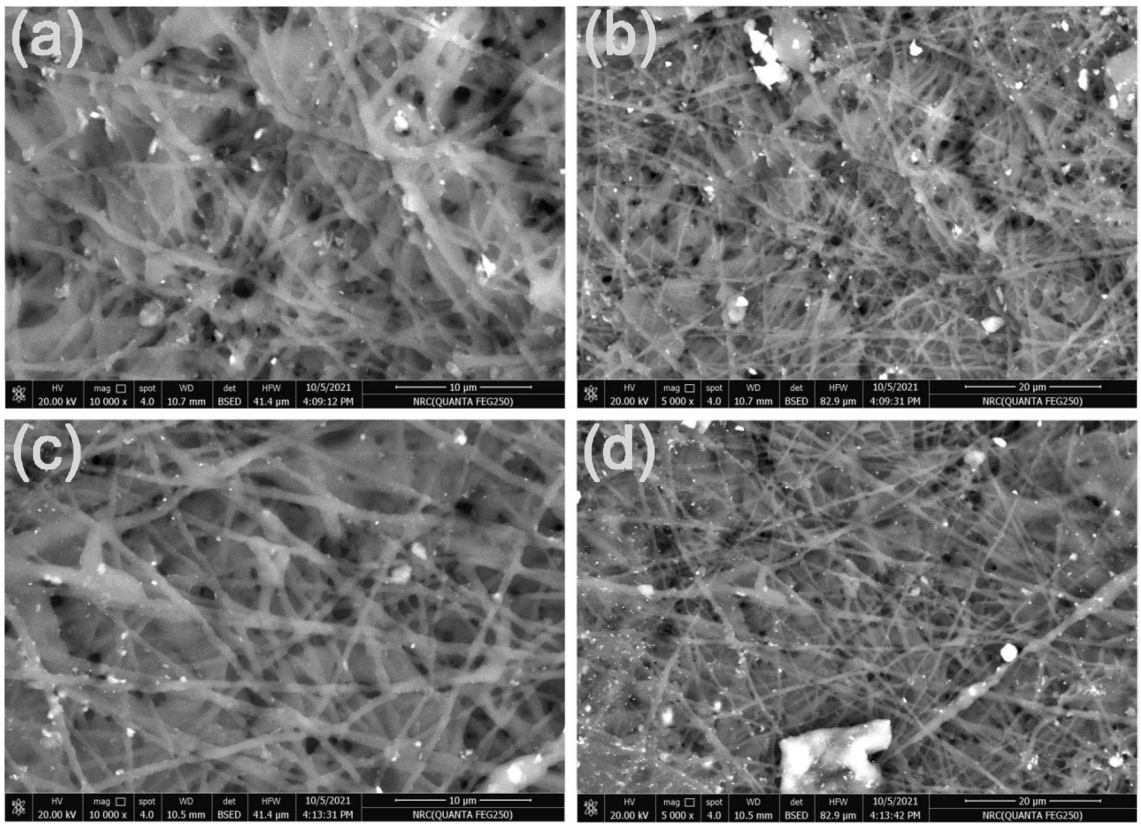

Fig. 6 SEM images of REAN@PET nanofibers; NF-0 (**a**, **b**), and NF-5 (**c**, **d**)

Dy were not noticeable by XRF as a result of their tiny concentrations. According to the results summarized in Tables 2 and 3, the elemental ratios employed in the preparation of both REAN and photochromic nanofibers were monitored to match the ratios of elements recognized by both EDX and XRF.

Figure 7 shows the FTIR curves used to validate the substitutions on the REAN@PET nanofibers. The aliphatic CH

Table 2 EDX analysis (elemental contents in wt%) of REAN@PET nanofibers at three different locations (L_1, L_2 and L_3) on the nanofibrous surface

LdAN@PET		C	O	Al	Sr	Eu	Dy
NF-0	L_1	61.22	38.78	Zero	Zero	Zero	Zero
	L_2	60.52	39.48	Zero	Zero	Zero	Zero
	L_3	61.39	38.61	Zero	Zero	Zero	Zero
NF-1	L_1	59.83	38.92	0.71	0.37	0.12	0.05
	L_2	59.86	38.87	0.64	0.39	0.18	0.06
	L_3	59.94	38.82	0.67	0.34	0.15	0.08
NF-3	L_1	59.26	38.71	0.93	0.60	0.38	0.12
	L_2	59.47	38.58	0.95	0.56	0.30	0.14
	L_3	59.31	38.54	1.06	0.68	0.31	0.10
NF-5	L_1	58.93	37.79	1.62	0.91	0.53	0.22
	L_2	58.92	37.87	1.58	1.02	0.42	0.21
	L_3	58.89	37.85	1.51	0.99	0.50	0.26
NF-7	L_1	57.94	37.50	2.21	1.23	0.73	0.39
	L_2	57.61	37.62	2.25	1.46	0.64	0.42
	L_3	57.86	37.78	2.18	1.03	0.81	0.34

Table 3 XRF analysis of the REAN@PET nanofibers

Element	Elemental content (wt%)			
	NF-1	NF-3	NF-5	NF-7
Al	50.76	53.39	55.15	57.31
Mg	4.28	3.20	2.28	0.83
Na	2.83	2.06	1.71	1.39
K	2.31	2.26	1.82	0.71
Ca	4.36	3.65	2.76	2.09
Cl	3.07	2.17	1.62	0.73
Si	5.57	4.68	3.06	2.48
Sr	26.82	28.59	31.60	33.46

stretch vibrations of the REAN@PET nanofibrous films resulted in an absorbance intensity of 2939 cm^{-1}. The OH stretch vibration can be assigned to the absorbance band at 3350 cm^{-1}, whereas the absorbance band of the carbonyl group stretch vibration was detected at 1715 cm^{-1} [38. The tetrahedron of Al–O with a symmetrical lattice structure is responsible for the distinctive bands at 467 and 771 cm^{-1}. The absorbance bands of $SrAl_2O_4$ almost completely buried suggesting that the absorbance bands of polyester overlap with the $SrAl_2O_4$'s primary characteristic bands. The absorption bands detected at 467, 564 and 771 cm^{-1} could be assigned to the crystal lattice vibrations of O–Al, O–Sr and O–Al–O, respectively [39]. The absorbance intensities of the hydroxyl and carbonyl groups observed at 3350 and 1715 cm^{-1} were monitored to decrease with raising the quantity of REAN to prove that the REAN aluminum ions acts as a coordination crosslinker between the polyester carbonyl and hydroxyl oxygen atoms on the polymer chains [39]. The REAN@PET nanofibers did not display any extra peaks as compared to the blank NF-0 nanofibrous film. Thus, the integration of REAN into the polyester fibrous bulk did not involve any chemical interactions.

Transparency and Mechanical Behavior

Rubbery REAN@PET nanofibrous films were created. The thickness of the film can be regulated by modifying the solution blowing spinning parameters. The REAN@PET film with a thickness of 25–35 μm demonstrated a mechanical stability. Greenish–yellow color emitted by the REAN@PET nanofiber films. Both flexibility and elasticity of REAN@PET were explored. The transparency of REAN@PET films is a notable property. The optical transmittance measurements were performed to verify the transparency of the film. The optical transmittance of the REAN@PET film would alter depending on the total amount of REAN in the polymer. The film optical transmittance decreased with increasing the REAN ratio. In comparison to NF-1, the NF-4 film had an optical transmittance of about 57%. The excitation wavelength detected at 365 nm proves the film transparency. The simple invisibility of a material has been significant for the preparation of efficient anticounterfeiting substrates. The REAN@PET films were tested for their mechanical properties by measuring their ability to stretch. A film rectangle that can be stretched up to 410% under varied tensile pressures has been reported. Equation (5) could be used to calibrate the elongation at the break [40].

$$\text{Elongation} = \frac{(L_a - L_o)}{L_o}, \tag{5}$$

where L_a is the tensile length, and L_o is the film length.

Elasticity and softness are often associated with greater elongation at break values. The REAN@PET elasticity

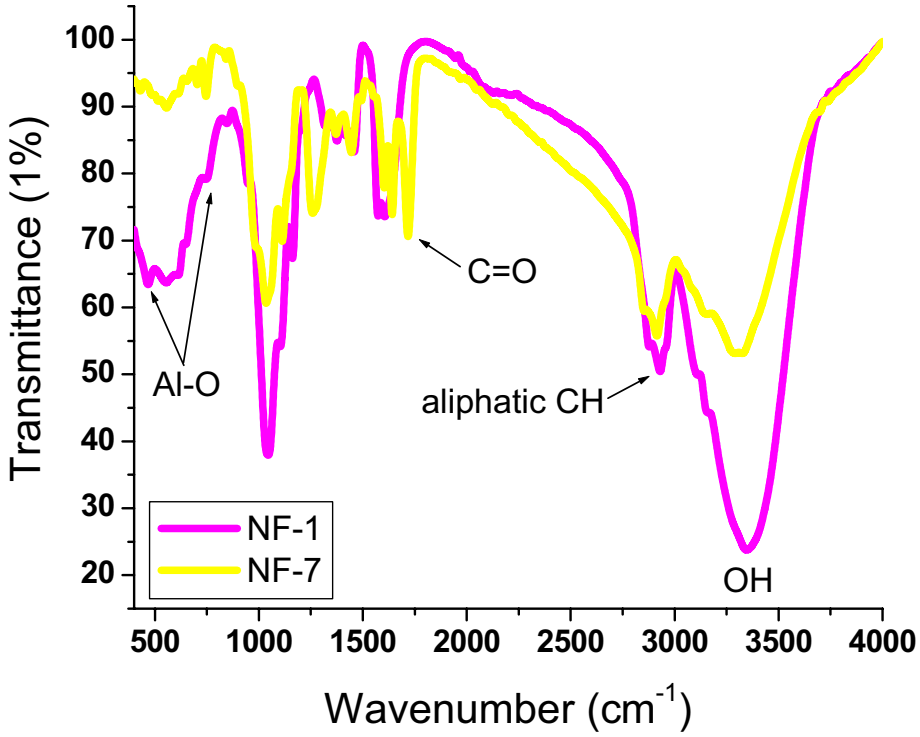

Fig. 7 FT-IR spectra of REAN@PET nanofibers

index was found to be 410% indicating a very high flexibility. A prominent emission at 519 nm was clearly monitored in the luminescence spectral curves under tension. A drop in the emission intensity at 519 nm was discovered to occur when the stretching elongation was increased due to the decreased REAN density in the film area underneath large strains. The stretch elongation did not affect the band location at 519 nm, indicating that the photoluminescence chromatic activities were not affected. Furthermore, the films can return to their original form after stretching, which demonstrates a high-quality elasticity and reusability for potential anticounterfeiting purposes, like packaging. The tensile strength of the REAN@PET film (NF-1) was lower than that of NF-0 (Fig. 8). Strain and tensile strength were shown to influence Young's modulus. Both tensile and Young's modulus decreased upon the insertion of REAN from NF-0 to NF-1. From NF-1 to NF-5, both Young's modulus and tensile increased with raising REAN, and then remained stable between NF-5 and NF-7. Negligible changes were detected in the strain owing to the full integration of REAN inside the nanofiber matrix. Interpolymeric strand bonding was enhanced by the use of REAN due to the improved coordination bond formation among the REAN Al positive ions and the partially negatively charged carbonyl and hydroxyl oxygen atoms on polyester. The tensile was improved when increasing the quantity of REAN till reaching NF-4; after that, it decreased owing to the increased space among the

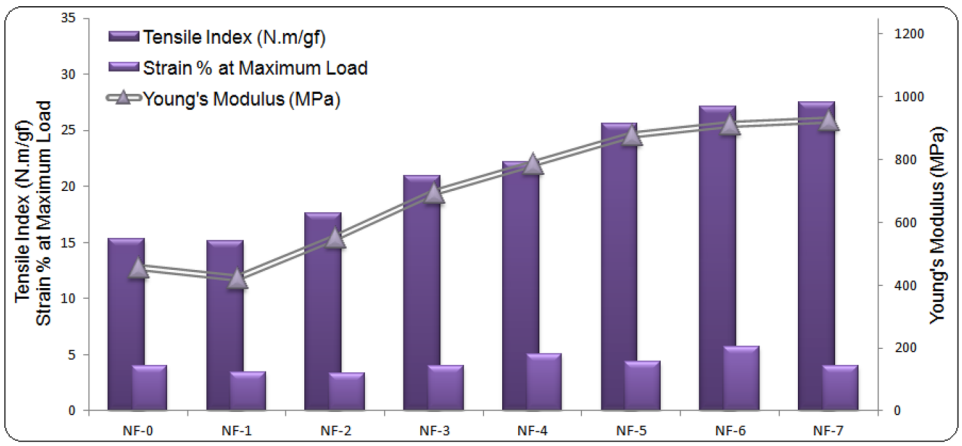

Fig. 8 Effect of REAN ratio on the mechanical properties of REAN@PET

Table 4 Hydrophobic screening of the REAN@PET nanofibers films

REAN@PET	Contact angle (°)	Slide angle (°)
NF-0	146.3	7
NF-1	149.1	7
NF-2	151.6	8
NF-3	153.8	9
NF-4	156.2	10
NF-5	157.8	11
NF-6	157.3	11
NF-7	156.7	12

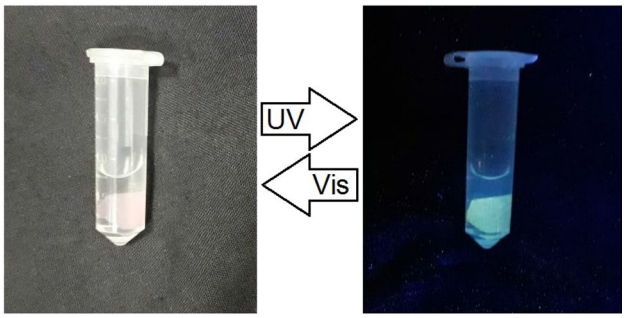

Fig. 9 Photochromism of NF-5 showing colorless shade under normal daylight (*left*), and green (*right*) emission under UV light

polyester strands owing to REAN coagulation between these polyester strands. Therefore, the tensile decreased at the REAN higher ratios.

Hydrophobic Properties

When the REA nanoparticles were included in the polyester matrix (NF-1), the nanofibrous film's contact angle increased from 146.3° (NF-0) to 149.1° (NF-1) as summarized in Table 4. The contact angle increased from 149.1° to 157.8° when the REA nanoparticles in the polyester matrix were increased from NF-1 to NF-5. In spite of this, the contact angle reduced marginally from 157.8° to 156.7° by increasing the ration of REAN from NF-5 to NF-7. Using larger concentrations of REAN improves the surface roughness. However, t is possible to reduce the surface roughness by further increasing the REAN density in the polyester bulk to result in decreasing the value of the static contact angle. The hydrophobic activity of the REAN@PET films was also evaluated using the sliding angle measurements. The PET nanofibers embedded with the REA nanoparticles show a shift in the wetting activity as the slide angle rises with increasing the REAN concentration. Figure 9 depicts the proof of the photochromic emission of NF-5 immersed in water.

Conclusions

Anti-counterfeiting REAN@PET nanofibrous films were made using the simple and green solution blowing spinning technology. The photochromic films were easy, quick, and affordable to make. Monitoring the REAN content at 1% ratio yielded the most fitting photochromic results. In the polyester nanofibrous film, the REAN are distributed within the fiber bulk in a homogenous manner, according to the morphology and chemical composition studies. The flexibility, transparency and elasticity were all characteristics of the prepared films. The stretching-rubber activity displayed stability with raising the tensile elongation magnitudes. REAN had a particle diameter between 4 and 9 nm, whereas REAN@PET had a fiber diameter between 180 and 220 nm. The structure of REAN was also proved by the XRD spectral analysis. An excitation peak monitored at 365 nm and an emission monitored at 519 nm were observed in the photoluminescent REAN@PET nanofibers. The hydrophobic characteristics of the REAN@PET nanofibrous films were enhanced with increasing the REAN ratio. The hydrophobic activity of the monitored nanofibrous films was enhanced, with contact angle values ranging from 146.3° to 157.8°. When exposed to UV light, the REAN@PET films produce a greenish-yellow pattern that is visible to the naked-eye. In contrast, this pattern is invisible under normal daylight. This is based on the photoluminescence spectra and colorimetric data from CIE Lab. A number of applications, including trademark protection, security printing, military camouflage, antireflective coatings, and optical electronics might benefit from the exceptional photostability and reversibility of the produced films.

Acknowledgements This project was supported by Researchers Supporting Project Number (RSP-2021/65), King Saud University, Riyadh, Saudi Arabia.

Funding Researchers Supporting Project Number (RSP-2021/65), King Saud University, Riyadh, Saudi Arabia.

Declarations

Conflict of interest The authors have not disclosed any competing interests.

References

1. Zhang Y, Yang H, Ma H, Bian G, Zang Q, Sun J, Zhang C, An Z, Wong W (2019) Angew Chem Int Ed 58:8773–8778
2. Ma T, Li T, Zhou L, Ma X, Yin J, Jiang X (2020) Nat Commun 11:1–8

3. Fukaminato T, Ishida S, Métivier R (2018) NPG Asia Mater 10:859–881
4. Wang L, Liu Y, Zhan X, Luo D, Sun X (2019) J Mater Chem C 7:8649–8654
5. Wei T, Jia B, Shen L, Zhao C, Wu L, Zhang B, Tao X, Wu S, Liang Y (2020) J Eur Ceram Soc 40:4153–4163
6. Huang G, Xia Q, Huang W, Tian J, He Z, Li BS, Tang BZ (2019) Angew Chem 131:17978–17983
7. Bretel G, Le Grognec E, Jacquemin D, Hirose T, Matsuda K, Felpin F-X (2019) ACS Appl Polym Mater 1:1240–1250
8. Chernov V, Salas-Castillo P, Díaz-Torres LA, Zúñiga-Rivera NJ, Ruiz-Torres R, Meléndrez R, Barboza-Flores M (2019) Opt Mater 92:46–52
9. Zhang L, Lyu S, Zhang Q, Wu Y, Melcher C, Chmely SC, Chen Z, Wang S (2019) Carbohydr Polym 206:767–777
10. Zhong R, Zhang J, Wei H, Qi X, Li M, Han X (2011) Chem Phys Lett 508:207–209
11. Nance J, Sparks TD (2020) Prog Org Coat 144:105637
12. Bierwagen J, Delgado T, Jiranek G, Yoon S, Gartmann N, Walfort B, Pollnau M, Hagemann H (2020) J Lumin 222:117113
13. Layani M, Kamyshny A, Magdassi S (2014) Nanoscale 6:5581–5591
14. Molavi F, Barzegar-Jalali M, Hamishehkar H (2020) J Control Release 320:265–282
15. Kausar A (2020) J Plast Film Sheeting 36:391–408
16. Zaghloul MYM, Zaghloul MMY, Zaghloul MMY (2021) Compos Struct 278:114698
17. Gao Y, Zhang H, Huang M, Lai F (2019) Constr Build Mater 228:116709
18. Kakati N, Assanvo EF, Kalita D (2019) J Polym Environ 27:2540–2548
19. Nodehi M (2022) Innov Infrastruct Solut 7:1–24
20. Liu L, Xu W, Ding Y, Agarwal S, Greiner A, Duan G (2020) Compos Commun 22:100506
21. Li Y, Zhu J, Cheng H, Li G, Cho H, Jiang M, Gao Q, Zhang X (2021) Adv Mater Technol 6:2100410
22. Bavatharani C, Muthusankar E, Wabaidur SM, Alothman ZA, Alsheetan KM, Al-Anazy M, Ragupathy D (2021) Synth Metals 271:116609
23. Atif R, Khaliq J, Combrinck M, Hassanin AH, Shehata N, Elnabawy E, Shyha I (2020) Polymers 12:1304
24. Abumelha HM (2021) Luminescence 36:1024–1031
25. Fichtner J, Watzele S, Garlyyev B, Kluge RM, Haimerl F, El-Sayed HA, Li W-J, Maillard FM, Dubau L, Chattot R (2020) ACS Catal 10:3131–3142
26. Abdelhameed MM, Attia YA, Abdelrahman MS, Khattab TA (2021) Luminescence 36:865–874
27. Khattab TA, Tolba E, Gaffer H, Kamel S (2021) Ind Eng Chem Res 60:10044–10055
28. Abou-Melha K (2022) Arab J Chem 15:103604
29. El-Newehy MH, Kim HY, Khattab TA, El-Naggar ME (2022) Ceram Int 48:3495–3503
30. El-Newehy MH, Kim HY, Khattab TA, Moydeen M, El-Naggar AME (2022) Luminescence 37:40–50
31. Khattab TA, El-Naggar ME, Abdelrahman MS, Aldalbahi A, Hatshan MR (2021) Luminescence 36:543–555
32. Khattab TA, Abd El-Aziz M, Abdelrahman MS, El-Zawahry M, Kamel S (2020) Luminescence 35:478–485
33. El-Newehy MH, Kim HY, Khattab TA, El-Naggar ME (2022) Luminescence 37:97–107
34. Valenta J (2018) AIP Advances 8:105123
35. Lin Y, Tang Z, Zhang Z, Wang X, Zhang J (2001) J Mater Sci Lett 20:1505–1506
36. Zhou D, Huang J, Liu J, Yan H, Zhang J, Zhang M, Liang G, Lu L, Zhang X, Xu P (2021) Solar RRL 5:2100112
37. Abumelha HM, Hameed A, Alkhamis KM, Alkabli J, Aljuhani E, Shah R, El-Metwaly NM (2021) ACS Omega 6:27315–27324
38. García PG, Ramírez-Aguilar R, Torres M, Franco-Urquiza EA, May-Crespo J, Camacho N (2018) Polymer 153:9–16
39. Mokhtar OM, Attia YA, Wassel AR, Khattab TA (2021) Luminescence 36(8):1933–1944
40. El-Newehy MH, Kim HY, Khattab TA, El-Naggar ME (2022) Development of highly photoluminescent electrospun nanofibers for dual-mode secure authentication. Ceram Int 48(3):3495–3503